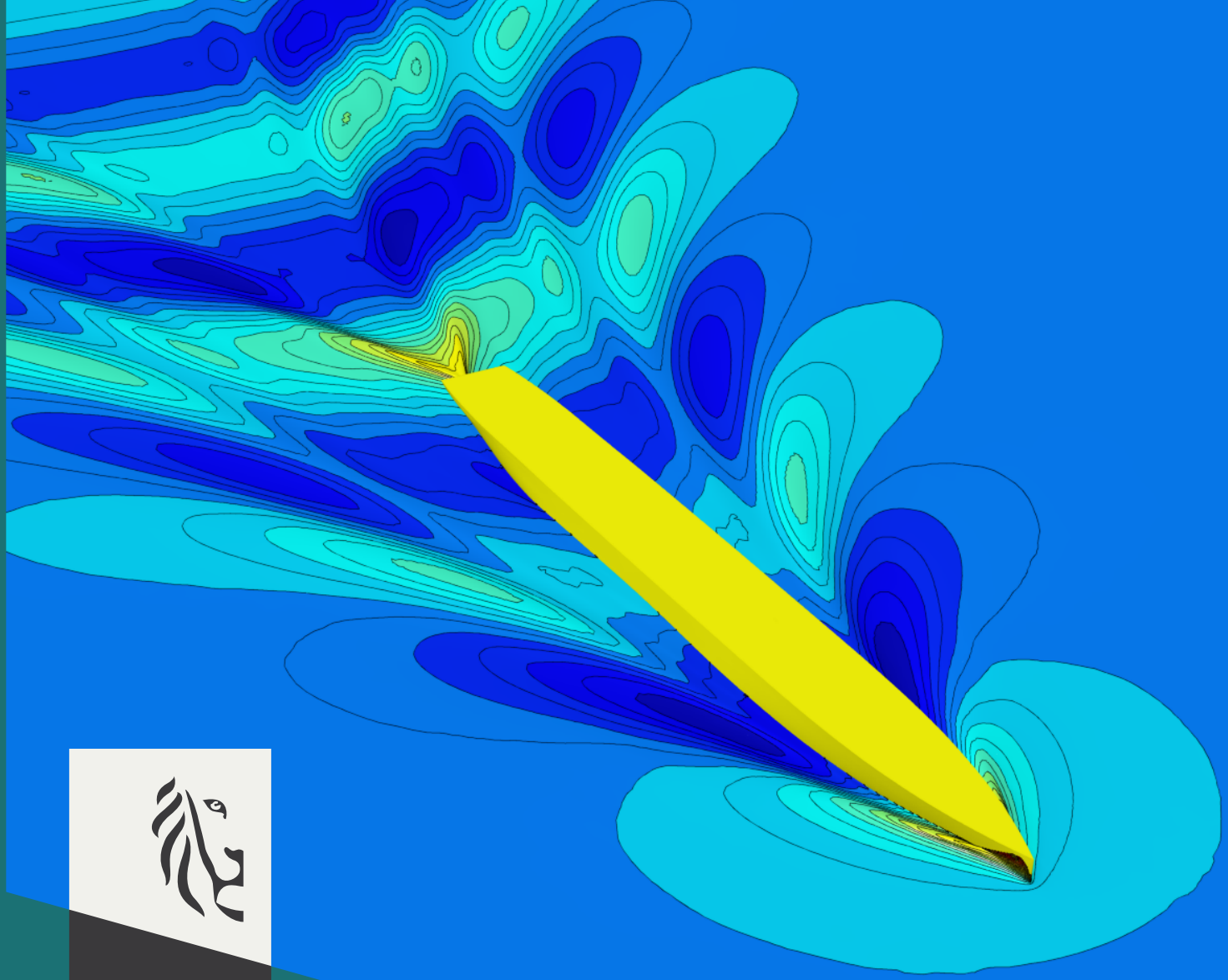

Flanders
State of
the Art

24_021_1
FH Reports

Model and Full-Scale Ship Resistance Prediction Workshop

DEPARTMENT
MOBILITY &
PUBLIC
WORKS

www.flandershydraulics.be

Model and Full-Scale Ship Resistance Prediction Workshop

Van Hoydonck, W.; Panahi, S.; López Castaño, S.

Flanders Hydraulics
Flanders State of the Art

Cover figure © The Government of Flanders, Department of Mobility and Public Works, Flanders Hydraulics

Legal notice

Copyright and citation

D/2025/3241/240

This publication should be cited as follows:

Van Hoydonck, W.; Panahi, S.; López Castaño, S. (2025). Model and Full-Scale Ship Resistance Prediction Workshop. Version 2.0. FH Reports, 24_021_1. Flanders Hydraulics: Antwerp

Document identification

Customer:	Flanders Hydraulics	Ref.:	WL2025R24_021_1
Keywords (3-5):	ship resistance prediction, model scale, full scale, CFD, FINE/Marine, workshop		
Knowledge domains:	Harbours and waterways > Resistance and propulsion > Open Water > Numerical calculations Harbours and waterways > Resistance and propulsion > Scale Effects > Numerical calculations		
Text (p.):	23	Appendices (p.):	0
Confidential:	No	☒ Available online	

Author(s):	Van Hoydonck, W.; Panahi, S.

Control

	Name	Signature
Revisor(s):	López Castaño, S.	Signed by:LOPEZ CASTAÑO Santiago Signed at:2025-09-19 16:19:16 +02:00 Reason:Ik keur dit document goed Vlaamse overheid
Project leader:	Van Hoydonck, W.	Signed by:Wim Van Hoydonck (Signature Signed at:2025-10-02 10:04:22 +02:00 Reason:Ik keur dit document goed Vlaamse overheid

Approval

Head of division:	Bellafkih, A.	Getekend door:Bellafkih Abdelkarim Getekend op:2025-09-17 19:30:37 +02:0 Reden:Ik keur dit document goed Vlaamse overheid

Abstract

In recent years, nautical research infrastructure (both towing tank and Computational Fluid Dynamics (CFD) tools) at Flanders Hydraulics (FH) are being used for the prediction of ship resistance in shallow and confined water, while in the past, the focus was mainly on the prediction of ship manoeuvring behaviour in these conditions.

To improve the confidence in and gain more experience with the numerical tools in use at FH for ship resistance prediction, FH participated in the model and full scale ship resistance prediction workshop organised by the JoRes consortium. The workshop aimed to compare numerical predictions of the resistance of the *Lucy Ashton* paddle steamer with experimentally obtained results at different model scales and at full scale. This report documents the work executed by FH during the participation of the workshop, the lessons learned and the knowledge gained.

Contents

List of Figures

List of Tables

Nomenclature

Abbreviations

CAD	Computer Aided Design
CFD	Computational Fluid Dynamics
DOF	Degree of Freedom
FH	Flanders Hydraulics
VOF	Volume-of-Fluid

Latin symbols

B	Breadth moulded	m
C_f	Friction coefficient	—
C_p	Pressure coefficient	—
D	Depth moulded	m
Fr	Froude number	—
g	Gravitational acceleration	$\mathrm{m/s^2}$
k	Turbulent kinetic energy	$\mathrm{m^2/s^2}$
L_{oa}	Length over all	m
L_{pp}	Length between perpendiculars	m
$L_{pp,m}$	Length between perpendiculars, model	m
$L_{pp,s}$	Length between perpendiculars, ship	m
L_{ref}	Reference length	m
T	Draft	m
t_a	Acceleration time	s
T_I	Turbulence intensity	—
U	Mean velocity	$\mathrm{m/s}$
u'	Root-mean-square of turbulent velocity fluctuations	$\mathrm{m/s}$
V_{ref}	Reference speed	$\mathrm{m/s}$

Greek symbols

∇	Displaced mass	kg
λ	Scale factor	—
μ_{air}	Air density	Pa s
μ_{water}	Water density	Pa s
ν_w	Kinematic viscosity	$\mathrm{m^2/s}$
ρ	Fluid density	$\mathrm{kg/m^3}$
ρ_{air}	Air density	$\mathrm{kg/m^3}$
ρ_{water}	Water density	$\mathrm{kg/m^3}$
τ_w	Viscous stress	$\mathrm{N/m^2}$

ω	Turbulent frequency rate	$1/\mathrm{s}$
ϵ	Dissipation rate	$\mathrm{m}^2/\mathrm{s}^3$

1 Introduction

1.1 Background

Understanding and minimizing ship resistance is crucial for designing vessels that are both more efficient and environmentally sustainable. Ship resistance significantly impacts fuel consumption, operational costs, and the overall carbon emissions of maritime operations. Traditionally, the investigation into ship resistance has relied on model-scale experiments. These experiments use scaled-down versions of ships to estimate the hydrodynamic performance of the full-sized versions, but they often struggle with accurately scaling the results due to the large differences in Reynolds number between model and full-scale ships and other scale-dependent factors.

The link between theoretical research and practical application has historically been bridged by such model-scale studies, yet the nuances of real-case scenarios often elude this traditional approach. As ships operate in open waters, they encounter a range of environmental factors and physical phenomena not fully reproducible in smaller-scale models. This discrepancy can lead to significant deviations between predicted and actual ship performance.

To address these discrepancies and better replicate real-world conditions, JoRes and Chalmers University of Technology have organized a workshop. This event marks the first occasion where data on ship resistance from full-scale experiments (excluding propeller effects), will be available. The unique aspect of the dataset of this workshop is the exclusion of the propeller in the full-scale experiments; consequently, experiments are more comparable to resistance tests rather than self-propulsion trials - which allow for a clearer understanding of the complex hydrodynamic characteristics of the vessel.

1.2 Objective

This report focuses on FH's contribution towards the above-mentioned project/workshop centred around the prediction of model- and full-scale ship resistance. To clarify further, the main objective of the workshop is to assess and compare CFD results from different participants for the prediction of the resistance of vessel at prototype scale, and to compare these results with existing full-scale experimentally obtained resistance data. The hull under investigation has also been tested at multiple towing tank facilities at multiple scale ratios in order to determine scale effects on the resistance.

As an important point, the workshop was designed to proceed blindly, meaning that the full-scale measurements were only disclosed after the workshop finished.

It is the intention of the workshop organisers to write a journal publication after the workshop using the data submitted by all participants, who will be added as coauthor in the publication.

1.3 Report Structure

Following a concise introduction that outlines the problem statement and the study's objective, the report contains the follow information:

In Chapter 2, all information required to setup and run the computations is given, starting with the hull geometry. It also elaborates on common settings and quantities of interest to the project. Finally, the conditions for the different simulation sets are given.

In Chapter 3, the computational setup in FINE/Marine for the different cases are described. This includes the setup of initial conditions, boundary conditions, mesh generation using HEXPRESS, and the simulation execution within FINE/Marine.

In Chapter 4, the results of the simulations are presented, focusing on metrics such as ship resistance, the wave pattern around the hull and outputs such as friction and pressure at requested locations on the hull. A detailed discussion follows, comparing the outcomes and interpreting their implications for different simulation sets.

Lastly, the conclusions drawn from this analysis are gathered in Chapter 5.

2 Simulation Specifications

2.1 Hull geometry

The geometry considered for this workshop is a ship hull whose main particulars are listed in Table 4. It (see Fig. 1) includes both the hull and the rudder, the latter of which must be retained in all CFD simulations. It should be noted that the geometry is provided at full scale with the origin of the coordinate system at the aft perpendicular, where the hull and the rudder surfaces join together, at the centre line of the vessel and at the keel.

Table 4 – Main characteristics of the hull.

Characteristic	Symbol	Value
Length between perpendiculars	L_{pp}	$58.1\,\mathrm{m}$
Breadth moulded	B	$6.4008\,\mathrm{m}$
Depth moulded	D	$2.1844\,\mathrm{m}$
Draft	T	$1.584\,\mathrm{m}$
Displaced mass	∇	$396.240\,\mathrm{kg}$

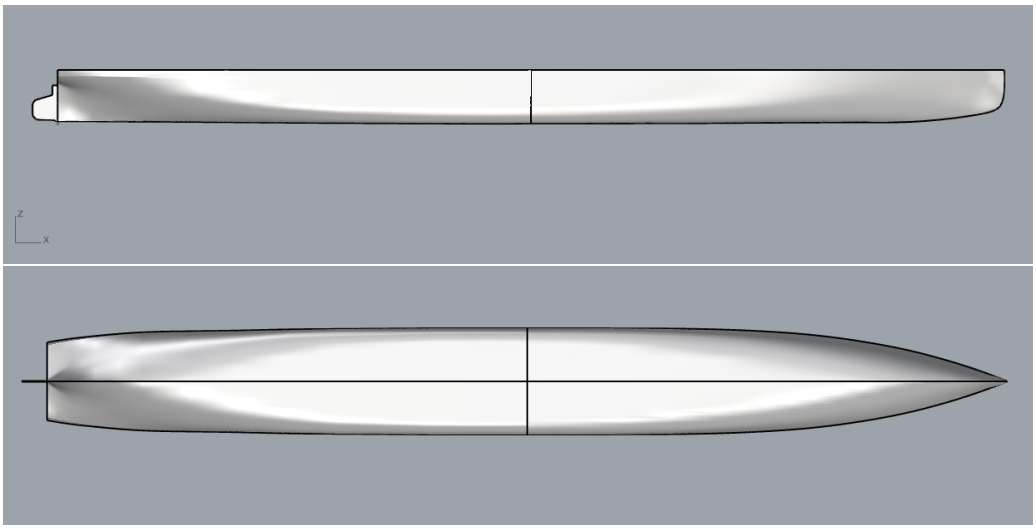

Figure 1 – Side view and bottom view of the hull of the *Lucy Ashton* paddle steamer as used for the workshop.

2.2 Common settings and quantities of interest

Physical properties are specified in Table 5 and Table 6 for the full-scale and model-scale simulations, respectively.

During the entire project, the hull is treated as hydrodynamically smooth: roughness is not used in the CFD computations. Concerning the specification of turbulence variables at the inlet, the workshop organisation has specified that the turbulence intensity T_I equals 1% and the turbulent viscosity ratio R_μ is 10.

Table 5 – Water and air properties for the full-scale simulations.

Property	Symbol	Value
Density (Air)	ρ_{air}	$1.225\,\mathrm{kg/m^3}$
Dynamic viscosity (Air)	μ_{air}	1.789×10^{-5} Pa s
Density (Water)	ρ_{water}	$1026.02\,\mathrm{kg/m^3}$
Dynamic viscosity (Water)	μ_{water}	1.22×10^{-3} Pa s
Gravitational acceleration	g	$9.81\,\mathrm{m/s^2}$

Table 6 – Water and air properties for the model-scale simulations.

Property	Symbol	Value
Density (Air)	ρ_{air}	$1.242\,\mathrm{kg/m^3}$
Dynamic viscosity (Air)	μ_{air}	1.77×10^{-5} Pa s
Density (Water)	ρ_{water}	$998.8\,\mathrm{kg/m^3}$
Dynamic viscosity (Water)	μ_{water}	1.27×10^{-3} Pa s
Gravitational acceleration	g	$9.81\,\mathrm{m/s^2}$

The following quantities must be delivered:

- Time history of the resistance, divided into friction and pressure components and given separately for the rudder, hull, and complete ship;
- Time history of the vertical force, divided into friction and pressure components;
- Time history of the side-force (for half of the hull), divided into friction and pressure components;
- Wetted surface area of the ship;
- Time-averaged transverse wave cuts at different longitudinal positions:
  - $x = -0.25\ L_{pp}$
  - $x = -0.1\ L_{pp}$
  - $x = 0$
  - $x = 0.25\ L_{pp}$
  - $x = 0.5\ L_{pp}$
  - $x = 0.75\ L_{pp}$
  - $x = 1.0\ L_{pp}$
- Time-averaged C_f and C_p cuts at different planes:
  - $x = 0.1\ L_{pp}$
  - $x = 0.25\ L_{pp}$
  - $x = 0.5\ L_{pp}$
  - $x = 0.75\ L_{pp}$
  - $x = 0.9\ L_{pp}$
  - One additional cut is requested along the centreline of the ship, along the keel.
- Time-averaged velocity profile on the boundary-layer at the centreline of the ship and two longitudinal positions:
  - $x = 0.49\ L_{pp}$
  - $x = 0.62\ L_{pp}$,

  along with the shear-stress at the wall for the corresponding position. The profiles should contain the velocity in the X-axis and the wall distance.
- Figures of the L_2 norm (RMS) of the residuals at the end of each time step for each of the solved variables. The Y-axis of the plot should be in logarithmic scale, ranging from 1 to 10^{-8}.

The friction (C_f) and pressure (C_p) coefficients are defined using

$$C_f = \frac{\tau_w}{0.5\rho_{water}{V_{ref}}^2}; \tag{1}$$

$$C_p = \frac{p - p_\infty - g\rho_{water}z}{0.5\rho_{water}{V_{ref}}^2}; \tag{2}$$

where τ_w is the viscous stress, p the total pressure and p_∞ the reference pressure.

2.3 Simulation sets

A total of 3 sets of simulations will be conducted. Detailed information about each simulation set is provided in the following subsections. In all computations, the $k-\omega\ SST$ (2003) turbulence model is used for closure of the RANS equations. This version of the model corresponds to that identified as SST-2003 in the NASA turbulence modelling resource.

2.3.1 Set 0

This set of simulations involves double-body simulations (without free surface) at full-scale for a single speed. A grid refinement study is conducted to ensure that the mesh configuration does not impact the final outcomes of the simulations. Structured grids are provided by the workshop organisation.

The simulations are carried out at a Froude number of 0.219, which equates to a velocity of $5.232\,\mathrm{m/s}$. All relevant quantities must be reported for each simulation, except for the wetted surface area and wave cuts, which are not applicable.

2.3.2 Set 1

This set consists of full-scale simulations at different speeds (and Froude numbers). The free surface must be included to account for wave-making effects. Workshop participants are required to generate their own grids and configure the cases using their own best practices. All quantities of interest are delivered for this set.

Mandatory part of the set:

- Fr = 0.130 (V_{ref} = $3.106\,\mathrm{m/s}$);
- Fr = 0.219 (V_{ref} = $5.232\,\mathrm{m/s}$);
- Fr = 0.304 (V_{ref} = $7.257\,\mathrm{m/s}$).

Optional part of the set:

- Fr = 0.173 (V_{ref} = $4.120\,\mathrm{m/s}$);
- Fr = 0.260 (V_{ref} = $6.211\,\mathrm{m/s}$).

2.3.3 Set 2

This set consists of simulations conducted at a fixed Froude number but with varying ship scales (and Reynolds numbers). Similar to Set 1, all simulations must include the free surface. All of the quantities of interest are reported for this set. The Froude numbers and scale ratios for each scenario are elaborated in Table 7.

For some of the smaller scales, the Reynolds number may justify the use of transition models. Hence, it may be necessary to use transition models to realistically replicate the simulations. Further details about the CFD setup will be provided in the following sections. The scale factor λ is defined as the ratio of the ship length to the model length:

$$\lambda = \frac{L_{pp,s}}{L_{pp,m}} \tag{3}$$

Mandatory part of the set:

- λ = 6.35 ($L_{pp,m}$ = 9.144 m);
- λ = 11.906 ($L_{pp,m}$ = 4.8768 m);
- λ = 21.167 ($L_{pp,m}$ = 2.7432 m).

Optional part of the set:

- λ = 7.938 ($L_{pp,m}$ = 7.3152 m);
- λ = 9.525 ($L_{pp,m}$ = 6.096 m);
- λ = 15.875 ($L_{pp,m}$ = 3.6576 m).

It should be noted that the above values for both scale λ and reference length $L_{pp,m}$ were supplied by the workshop organisation. A quick check shows that these values are only accurate to the third digit. E.g. for $\lambda = 11.906$, it follows that $L_{pp,m} = \frac{lpp}{\lambda} = \frac{58.1\,\text{m}}{11.906} = 4.879\,89\,\text{m}$ and not the value ($4.8768\,\text{m}$) as shown above. All model scale reference length values as supplied by the workshop organisation suffer from these inaccuracies. The reverse computation (multiplying $L_{pp,m}$ with its corresponding λ) gives, at full scale, $L_{pp} = 58.0632\,\text{m}$, and similar values are found for the other scales, from which one can conclude that the full-scale reference length is likely inaccurate.

Something similar seems to happen with the velocity values for Set 1: the Froude numbers and associated velocities do not match exactly. The values of the scales have been used to compute numerically the corresponding reference length (which therefore may have an offset of some millimeters).

Table 7 – Test matrix overview.

	Fr				
λ	0.130	0.173	0.219	0.260	0.304
1	S1 Req.	S1 Opt.	S0, S1, & S2 Req.	S1 Opt.	S1 Req.
6.35	×	×	S2 Req.	×	×
7.938	×	×	S2 Opt.	×	×
9.525	×	×	S2 Opt.	×	×
11.906	×	×	S2 Req.	×	×
15.875	×	×	S2 Opt.	×	×
21.167	×	×	S2 Req.	×	×

The scaled-down versions of the domains are generated by resizing the full-scale domain with the factor $1/\lambda$. The numerical values are presented in Table 8.

2.4 Inlet turbulence parameters

The turbulence intensity T_I is defined as

$$T_I = \frac{u'}{U}, \tag{4}$$

Table 8 – Scale factors

λ	$1/\lambda$	V_{ref} / m/s	L_{ref} / m
1.0000	1.0000	5.2320	58.100
6.3500	0.157 48	2.0763	9.1496
7.9380	0.125 98	1.8570	7.3192
9.5250	0.104 99	1.6953	6.0997
11.906	0.083 991	1.5163	4.8799
15.875	0.062 992	1.3131	3.6598
21.167	0.047 243	1.1372	2.7448

where u' is the root-mean-square of the turbulent velocity fluctuations and U is the mean velocity, taken as the ship speed. The turbulent kinetic energy k is related to T_I and U by

$$k = \frac{3}{2}(T_I U)^2. \tag{5}$$

The user interface of FINE/Marine requires values for the dissipation rate ϵ,

$$\epsilon = C_\mu \frac{k^2}{R_\mu \nu_w}, \tag{6}$$

where ν_w is the kinematic viscosity (of water). The turbulent frequency rate ω can be computed from

$$\omega = \frac{k}{\nu_w R_\mu} \tag{7}$$

For the full scale computations listed in Table 7, values for the turbulent quantities required by FINE/Marine are shown in Table 9.

Table 9 – Turbulent quantity values

V_{ref} / m/s	k / m^2/s^2	ϵ / m^2/s^3
3.1060	0.001 447 1	0.015 850
4.1200	0.002 546 2	0.049 069
5.2320	0.004 106 1	0.127 61
6.2110	0.005 786 5	0.253 44
7.2570	0.007 899 6	0.472 33

3 Computational setup

3.1 Set 0 - double body computations

3.1.1 Domain geometry

For this set of computations, the workshop organisation delivered five structured grids in the following three formats exported from Pointwise:

- `cgns`;
- `pointwise`;
- `starccm`.

`Grid1` is the finest grid and `Grid5` is the coarsest. Fig. 2 shows for the coarsest computational grid a view of the domain topology and the cells on the inlet and both mirror planes. The dimensions of the computational domain are based on the characteristic length of the vessel: L_{pp} = 58 m. The quarter-circular domain inlet has a radius of $1L_{pp}$, the inlet is located $1L_{pp}$ ahead of the bow of the vessel and the outlet is located 125 m aft of the stern ($\approx 2.2L_{pp}$). This is significantly smaller than the domain sizes used at FH for shallow water computations.

The grid sizes for the five domains are recorded in Table 10.

Table 10 – Cell count for the supplied grids in Set 0.

Grid no.	cell count
1	34 114 300
2	21 506 560
3	12 557 952
4	6 347 956
5	2 688 320

Importing the *cgns* grids in Hexpress resulted in an error because Hexpress does not support multiblock cgns grids. This issue was reported to Cadence[1] and a workaround was provided using the following steps:

- Import the `cgns` file in `iggmarine` version 121-4;
- Save the project (which creates an `*.igg` project file);
- Open this `*.igg` file with Hexpress as usual.

In addition to the above issue, a second support case (46 792 610) was opened to report formatting issues in the output of the grid conversion.

3.1.2 Computational setup

These five deep-water computations were initially configured as unsteady, single-phase computations with two mirror planes. This worked well for the coarsest grid (Grid 5) and the three finest grids (1, 2 and 3), but Grid 4 failed to converge (see Fig. 3).

[1] The support case number was 46 792 329.

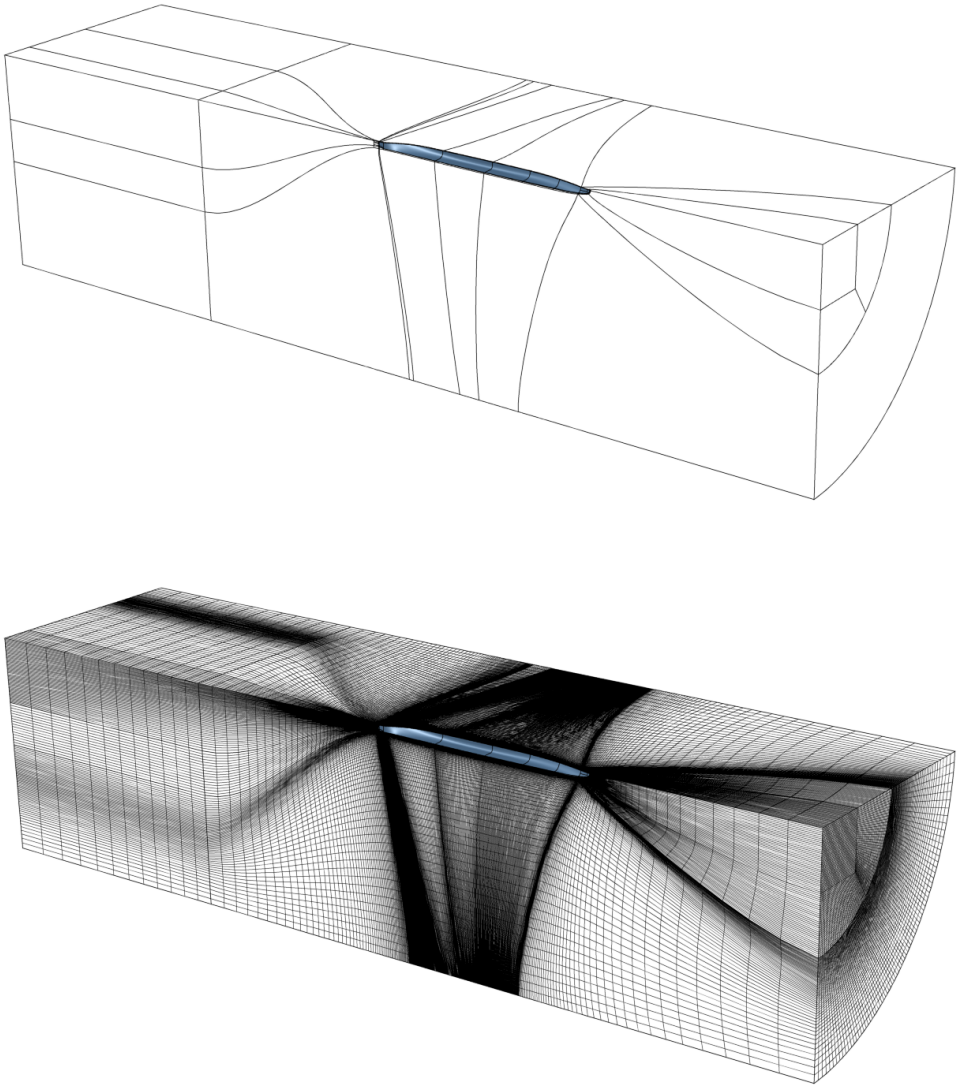

Figure 2 – View of the domain with domain patches (top) and cells (bottom) for the coarsest grid.

For this type of computations, the documentation mentions two possibilities for the computational setup: one where a single phase computation is used, and a second method using a two-phase setup. For the latter, the free surface must be located above the top surface of the computational domain and the under-relaxation parameter for the mass fraction (numerical schemes) should be set to a negative value. This ensures that the mass fraction equation is not updated during the computation. The height of the free surface was set to 10.0668 m, which results in a hydrostatic pressure at the free surface that is similar to the atmospheric pressure at sea level. Modifying the single-phase setup to a two-phase setup resulted in converging computations for all five grids (see Fig. 4). After the workshop, Cadence added a section to the *Best Practices* for single-phase resistance computations related to the use of structured grids (probably because they received one or more support requests related to the computations in Set 0 of the workshop). Structured grids consisting of multiple patches may have areas with significant cells clustering and larger expansion ratios than unstructured grids. Such grids can lead to stability issues for the flow solver. The recommended changes are: In the *Control variables*, set the `gradEvaluation_` expert parameter to `GAUSS METHOD - CORRECTIONS` (default: `GAUSS METHOD + CORRECTIONS`); In the *numerical models*, modify the under-relaxation parameters for the 3 components of the velocity from 0.5 to 0.2.

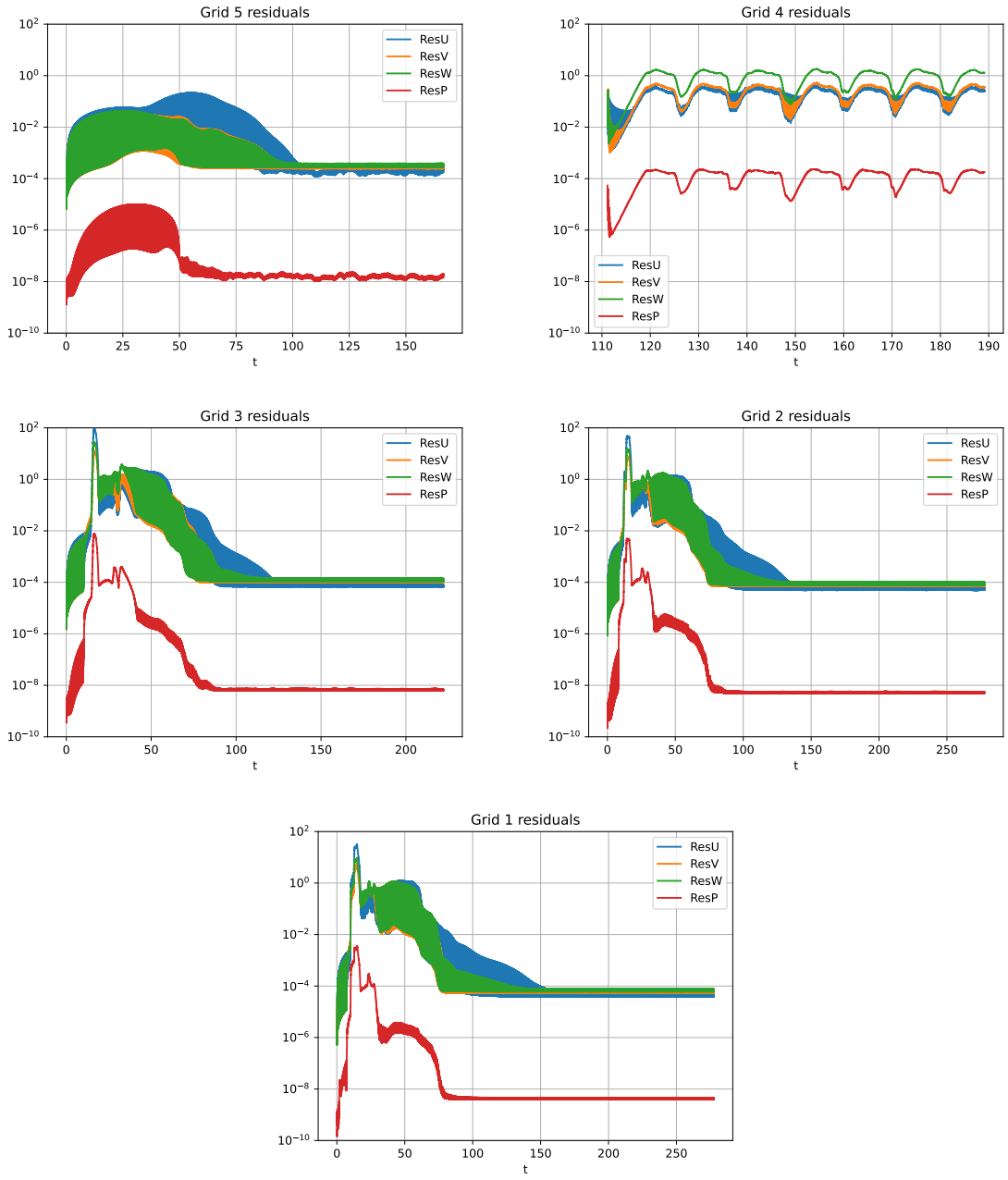

Figure 3 – Visualisation of residuals for the five computations in Set 0 with a single-phase setup: Set 4 (second coarsest grid) failed to converge.

While writing this report, extra (steady single phase) computations were configured with these settings for all computations in Set 0 which indeed shows that the instabilities are removed (compare the data in Fig. 5 with the results of Grid 4 shown before in Fig. 3). The differences in results between the two setups will be discussed as well.

The reference length and reference speed for these computations are $58.1\,\mathrm{m}$ and $5.232\,\mathrm{m/s}$, respectively. The gravitational acceleration is set to $9.81\,\mathrm{m/s^2}$ and as mentioned before, the turbulence model is $k\omega$ (SST-Menter-2003).

Boundary conditions are set as follows: wall functions are used on the hull and rudder surfaces. The inlet and cylindrical side of the domain are assigned the *Far field* boundary condition with the velocity components set to 0. The turbulent kinetic energy and dissipation are set to the values as discussed in § 2.4. At the outlet,

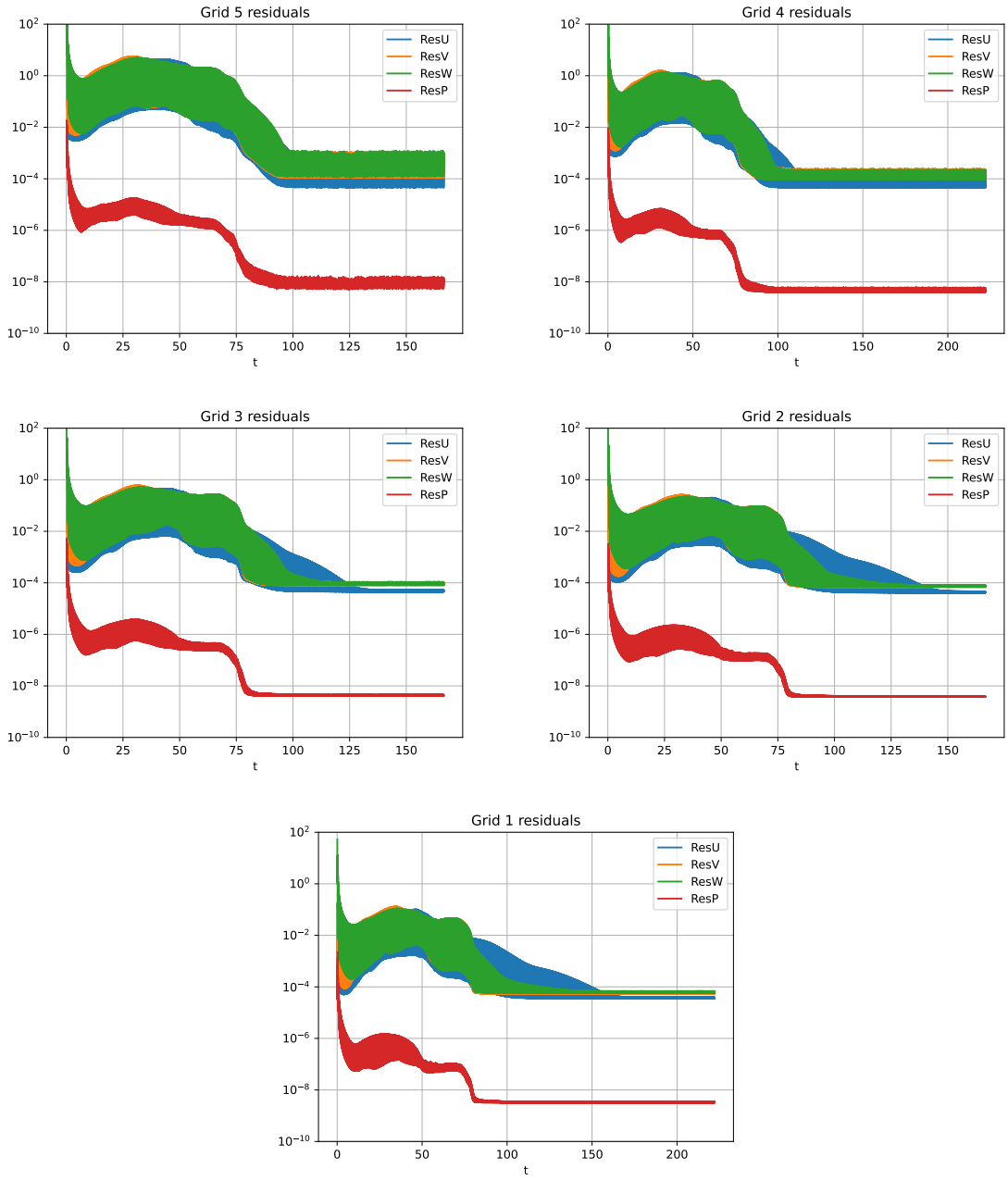

Figure 4 – Visualisation of residuals for the five computations in Set 0 with a two-phase setup as used for the submission.

the pressure was set to *Frozen pressure* and for both mirror surfaces (symmetry plane and plane at the free surface), the mirror boundary condition is used.

The hull and rudder patches are combined in a single body named *hull* and the patches defining the rudder are additionally combined in a sub-body such that the solver can compute forces on it separately. Motion is applied to the hull by defining a motion law for its longitudinal Degree of Freedom (DOF) `Tx0`. For this, a sinusoidal ramp is used with a duration of $t_a = 50\,\mathrm{s}$ in which the speed increases from $0\,\mathrm{m/s}$ to the reference speed of $5.232\,\mathrm{m/s}$. The reference point for the forces computation is set to the midship position ($x = 29.05\,\mathrm{m}$) at the free surface location ($z = -1.6742\,\mathrm{m}$). The mesh displacement definition is set to rigid motion for `Tx0` where the rigid motion is copied from the hull. The solver is run for at most 2000 time steps with a stepsize $\Delta t = 0.111\,047\,4\,\mathrm{s}$.

The workshop organisation required averaged flow field variables. Averaging was started after $110\,\mathrm{s}$ for the

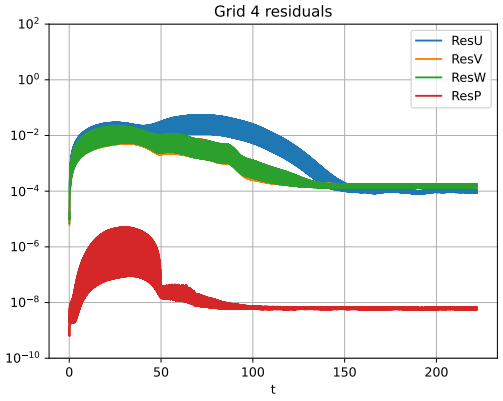

Figure 5 – Visualisation of residuals for grid 4 in Set 0 with a single-phase steady setup with solvers settings adapted for structured grids.

following fields:

- Pressure;
- Viscous stress (fluid to wall);
- Velocity;
- Vorticity;
- Turbulent kinetic energy;
- Correlation R11, R22 and R33.

3.2 Set 1 and 2 - free surface computations

3.2.1 Domain geometry

Fig. 6 shows the side view of the computational domain that is shaped as a rectangular cuboid. The overall length of the hull (rounded up to 60 m) is used as a basis to determine the domain size. The bow is located $3L_{oa}$ from the inlet, while the outlet is located $4L_{oa}$ aft of the stern. The interface between the air and water phase is located at $z = 0$ m, the domain bottom is located $2.5L_{oa}$ further down and the domain top is located $1.5L_{oa}$ above the water surface. For the current computations, the starboard side of the hull is retained and the lateral side of the domain is located $3L_{oa}$ from the symmetry plane. In absolute values, the computational domain has a length of 480 m, a width of 180 m, and a height of 240 m. For the model scale computations in Set 2, the domain and hull will be scaled down using the scale factors in Table 7. The x-axis of the global axes system points towards the bow, the Y-axis points towards port and the Z-axis points upwards.

The topology of the hull is adapted from the default, where most changes are related to the surfaces that define the rudder width: patches are only retained if faces are joined with a sharp angle. As a result, the rudder consists of one side surface and three trailing edge surfaces. Likewise, edges along the rudder outline are merged where they join smoothly. The surfaces defining the hull front and rear halves were merged and both edges that run from bow to stern were merged. The edge at the keel was subsequently split in three parts so that the hull areas near the bow and stern could be refined separately from the rest of the hull. Near the bow, the split is located at $x = 24.07$ m and at the stern, it is located at -21.8 m.

These modifications result in one *hull* surface, one *deck* surface, one *transom* surface, three *rudder trailing edge* surfaces and one *rudder side* surface for meshing.

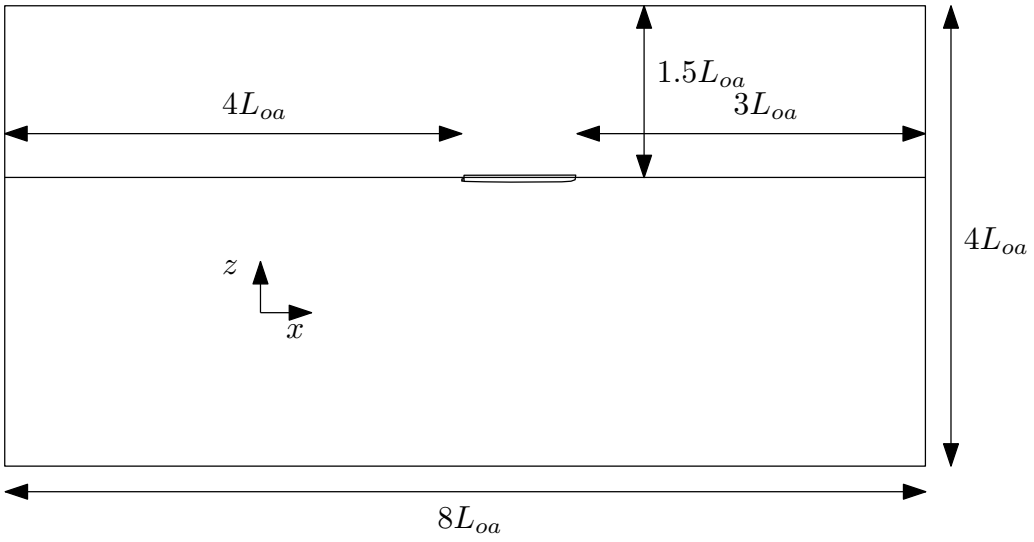

Figure 6 – Overview of the computational domain for simulations.

3.2.2 Mesh generation

The unstructured hexahedral grid generator HEXPRESS is used to produce all grids for Set 1 and 2. For Set 1 (influence of speed on resistance), two meshes have been created, one for higher speeds and one for lower speeds. The differences are only related to the viscous layer settings and will be discussed at the end of this subsection. After finishing the computations for Set 1, the computations for Set 2 were configured by duplicating one of the projects of Set 1 and scaling the domains and absolute mesh settings with the scale factor λ and scaling all dimensional quantities such as the reference velocity, reference speed, reference time and turbulence values.

3.2.2.1 Initial mesh

For the initial Cartesian mesh, the domain is divided in 32 cells in the X-direction, 12 cells in the Y-direction and 16 cells in the Z-direction. As such, the resulting cells are cubic with linear dimensions 15 m, which corresponds to a relative cell size of $L_{pp}/4$.

3.2.2.2 Mesh refinement

The smallest linear dimension of the hull's Computer Aided Design (CAD) model is the width of the (half) rudder, which is $0.022\,26$ m. Table 11 contains absolute values of cell edge length as a function of the refinement level. It follows that a maximum refinement level of 10 is sufficient to capture the smallest edges.

The global refinement diffusion is increased to four (from its default value of two).

The three rudder trailing edge surfaces are assigned 10 refinements, while the rudder side is refined eight times. The hull is uniformly refined seven times, the deck five times and the transom six times.

The topological curves in the domain are not used for refinement with the exception of the following four curves:

- the curve located at the symmetry plane of the transom: seven refinements;
- the curve connecting the rudder side to the hull: nine refinements;
- the front hull curve in the symmetry plane of the hull starting near the bow: nine refinements;
- the aft hull curve in the symmetry plane of the hull: nine refinements.

Table 11 – Cartesian cell sizes as a function of refinement level.

Subdivision level	Cell size
0	15.000
1.0000	7.5000
2.0000	3.7500
3.0000	1.8750
4.0000	$0.937\,50$
5.0000	$0.468\,75$
6.0000	$0.234\,38$
7.0000	$0.117\,19$
8.0000	$0.058\,594$
9.0000	$0.029\,297$
10.000	$0.014\,648$
11.000	$0.007\,324\,2$

In addition to these adaptations, two refinement boxes and one sector are defined to add additional refinement: a hull refinement below the waterline (non-volumic, eight refinements); hull wake refinement (volumic, seven refinements) in a box with cross sectional dimensions equal to the hull draft and hull width, extending 14 m aft of the stern and a length of 27 m and Kelvin wake refinement (volumic, eight refinements) with target cell sizes 0.5625 m, 0.5225 m and $0.070\,312\,5$ m that extends approximately $1L_{pp}$ aft of the stern. The origin of the refinement sector is located at 36.62 m, 0.0 m and -0.2905 m. For the Kelvin wake refinement, the target cell sizes in x- and y-direction are approximately equal to $\frac{L_{pp}}{100}$, while in the z-direction, cells are refined up to $\frac{L_{pp}}{1000}$.

Fig. 7 provides a top view of the volumic refinement boxes discussed above[2].

3.2.2.3 Viscous layers

As for the current project, hull resistance prediction is the primary goal, no wall functions are used: a low $Y+$ value (0.8) is selected for the hull and rudder surfaces. Two meshes are created, one for the highest speeds, and the second one for the lower speeds. The settings related to the viscous layers specific to the high speed and low speed cases are listed in Table 12 together with the grid sizes after viscous layer insertion. The surface mesh at the bow and stern of the hull is shown in Fig. 8 where also, a cross section at the midship location is shown.

Table 12 – Viscous layer settings for the high and low speed cases.

Case	Reference speed	y_{wall}	total cell count
Low speed	$4.12\,\mathrm{m/s}$	1.386×10^{-5} m	7.439×10^{6}
High speed	$6.211\,\mathrm{m/s}$	9.681×10^{-6} m	7.660×10^{6}

3.2.3 Adaptations for Set 2

As discussed before, the computations for Set 2 consist of a single velocity at different scales. One full-scale computational setup from Set 1 is duplicated and scaled down to the correct size. The absolute mesh settings (such as those related to the water surface refinement and viscous layers) are adapted accordingly. For the

[2]The refinement box for the underwater part of the hull is not shown as its sizes do not really matter

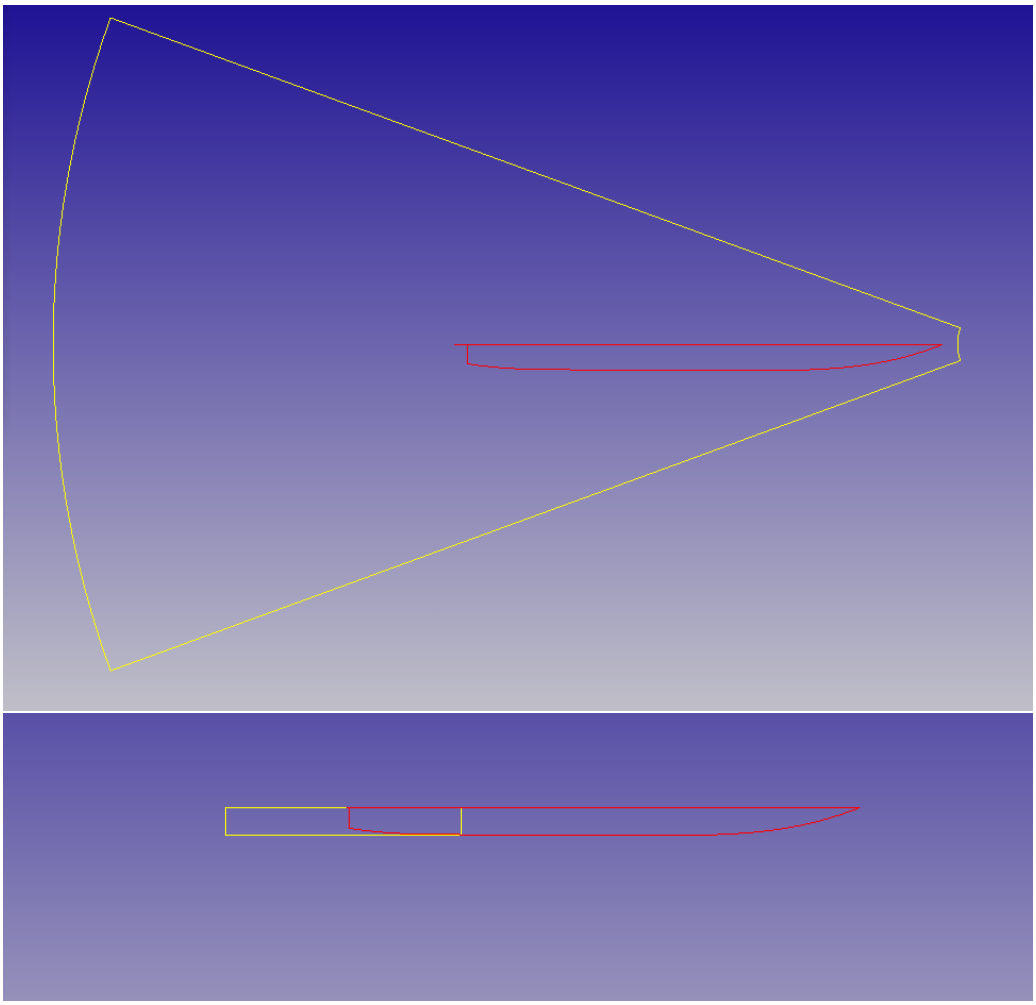

Figure 7 – Volumic refinement boxes for the Kelvin wake (top) and hull wake (bottom).

viscous layer settings, the same value for $Y+$ is used for all scales (0.8) and as the model size is reduced, the relative thickness of the boundary layer increases, resulting in a reduction of the grid size, as shown in Table 13.

Table 13 – Grid sizes for the computations in Set 2 at different scales λ.

λ	total cell count
6.35	$8\,337\,642$
7.938	$6\,001\,193$
9.525	$5\,781\,929$
11.906	$5\,566\,325$
15.875	$5\,346\,780$
21.167	$5\,226\,042$

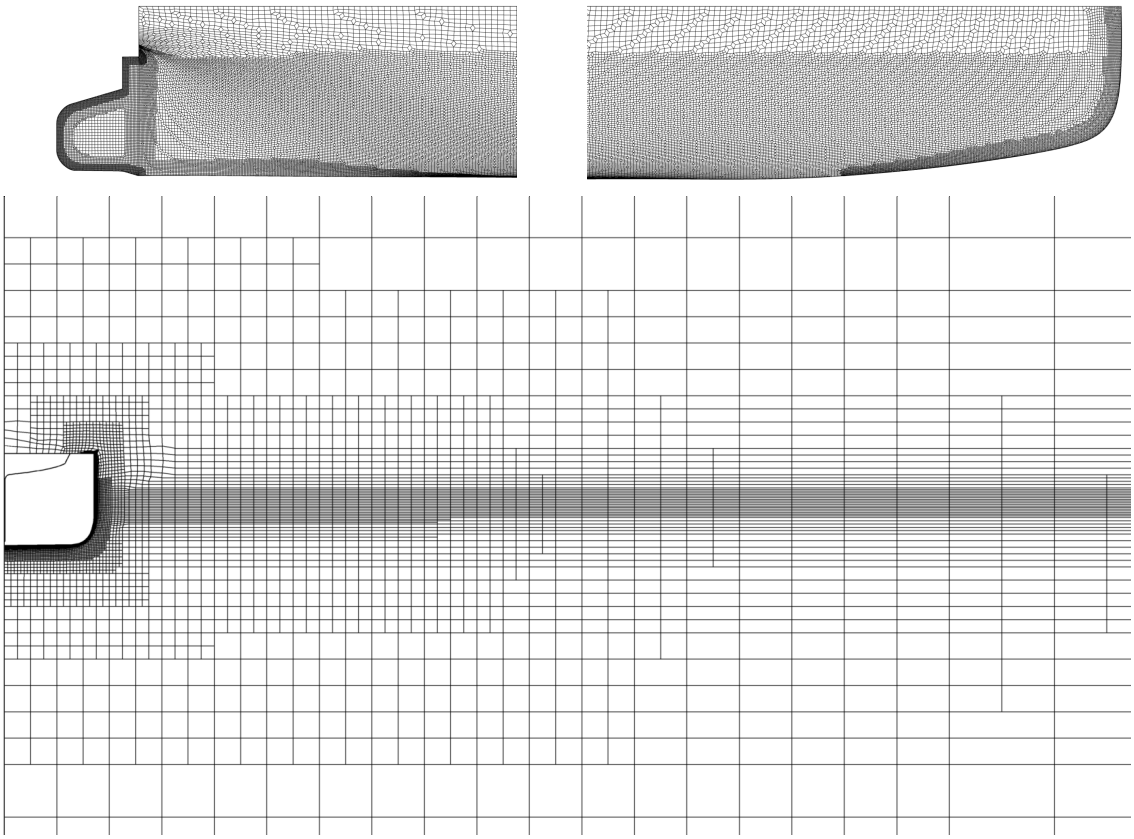

Figure 8 – Sideview of the hull near the stern (top left), bow (top right) and a lateral cross section near the midship location (bottom).

3.3 Numerical setup

3.3.1 Fluid properties and boundary conditions

A two-phase Volume Of Fluid (VOF) ansatz is used where the specifications of water and air are defined in § 2.2. The flow is presumed to be fully turbulent and the $k-\omega\ SST$ (2003) turbulence model is utilised for numerical simulations. The reference length is set to 58.1 m and the reference velocity varies as listed in Table 7.

The hull surfaces are defined by a Wall-function boundary condition, except for the deck surface, which uses a Slip condition (zero shear stress).

Both top and bottom of the domain are set to *prescribed pressure - updated hydrostatic pressure*, while the domain sides utilise a *Far field velocity* condition with all velocity components set to zero.

3.3.2 Body motion and mesh management

The patches forming the hull are grouped into a single body to enable the application of motion laws. For this project, the body is divided into two sub-bodies (hull and rudder), to compute forces on both sub-bodies separately (as requested by the workshop organisation).

The longitudinal motion ($\mathrm{Tx}0$) is imposed and the remaining DOFs are fixed (no trim nor sinkage). At the start of a simulation, the longitudinal velocity is smoothly (1/2 sinusoidal ramp) increased from $0\,\mathrm{m/s}$ to the target velocity during a period of $50\,\mathrm{s}$.

For computations with this type of motion definition, a rigid motion mesh deformation boundary condition is

assigned to the imposed motion component (`Tx0`).

3.3.3 Initial solution

Initial conditions for the field variables are required. The initial velocity in all directions is set to zero, compatible with the motion definition of the hull ($V = 0\,\mathrm{m/s}$ at $t = 0\,\mathrm{s}$). Initial values for the turbulence quantities are adapted to correspond to the values as detailed in § 2.4. In the context of two-phase flow computation, the position of the fluid interface is also established and set to zero.

3.3.4 Numerical parameters

The default discretization schemes are used for the different transport equations: `AVLSMART` for both *turbulence* and *momentum* and `BRICS` for *multi-fluid*. The theoretical background for these choices is explicated in the FINE/Marine Theory Guide.

The under-relaxation parameters are left at their default values. The streaking correction and velocity clipping options were activated for the computations.

3.3.5 Solver settings

The time step law is set to uniform, with a time step value that depends on the desired hull speed as follows:

$$\Delta t = \frac{1}{100}\frac{L_{ref}}{V_{ref}}, \tag{8}$$

For instance, for $V_{ref} = 6.211\,\mathrm{m/s}$, $\Delta t = 0.093\,544\,\mathrm{s}$. Computations are conducted for a fixed number of time steps (up to 4000).

A maximum of eight non-linear iterations is executed during each time step. This value is reduced if the solver can reduce the residuals by two orders in less iterations.

3.3.6 Adaptations for Set 2

For the computations in Set 2, the reference length and reference speed are reduced. The final velocity in the motion definition is adapted as is the time period for the acceleration phase of the computations. The latter one is Froude-scaled using $\sqrt{\lambda}$. As an example, the acceleration time for the computation at $\lambda = 11.906$ equals $t_a = 14.5\,\mathrm{s}$. Initial values in the domain and boundary values for turbulence quantities are scaled using the equations in § 2.4.

4 Results and Discussions

In this chapter, some results as requested by the workshop organisation are discussed.

4.1 Set 0

In Fig. 9, a comparison is shown of the pressure, viscous and total drag of the hull for both the two-phase and single-phase computations for Set 0. The horizontal axes represents the grid, with grid 1 the finest and grid 5 the coarsest grid. As the grid is refined, the resulting viscous resistance for the two-phase setup converges significantly slower than the one-phase setup, which has a slightly smaller (absolute) value.

The difference between the two setups for the pressure setup is significant. Due to the use of two Volume-of-Fluid (VOF) phases, the pressure at the top surface for the two-phase computation depends on the location of the free surface. As stated before, this was placed such that the pressure at the free surface corresponds to standard atmospheric pressure (this value was also submitted to the workshop organisation). For the single phase setup, the pressure at the top cannot be set explicitly by the user. By default, the solver outputs both (total) pressure and hydrodynamic pressure, the latter of which is the total pressure minus the hydrostatic pressure. For the workshop, the forces on the hull were requested, for which the solver does not make the distinction between total pressure and hydrostatic pressure. The only possibility was to submit the total pressure force, which is about 500 times higher than what it should be.

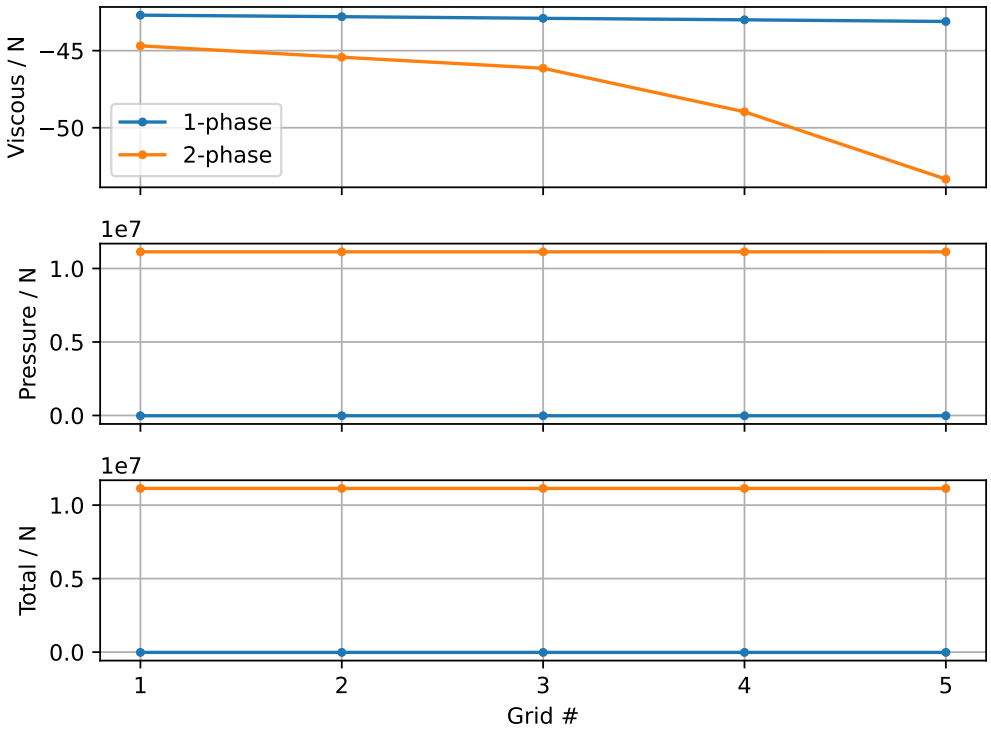

Figure 9 – Comparison of predicted resistance as a function of the grid for the computations using a single phase and two-fase setup.

4.2 Hull forces - Set 1 and 2

The three components of the resultant hull force (longitudinal, lateral and vertical) for Set 1 are gathered in Fig. 10. For the resistance (longitudinal or X-component), both the total force as well as its pressure and viscous contributions are shown. This division is not shown for the lateral and vertical force components, as the viscous contribution in those cases is nearly zero. Results are shown as dimensionless quantities, by dividing the dimensional results with $\frac{1}{2}\rho {V_{ref}}^2 L_{ref} T$. The viscous component of the resistance is almost independent from the speed, with slightly higher values at lower speeds. At low speeds, the pressure resistance contribution is significantly lower (less than half) than the viscous contribution, while at the highest speed, its contribution is slightly higher. Both the lateral and vertical hull forces show a decreasing trend with increasing speed.

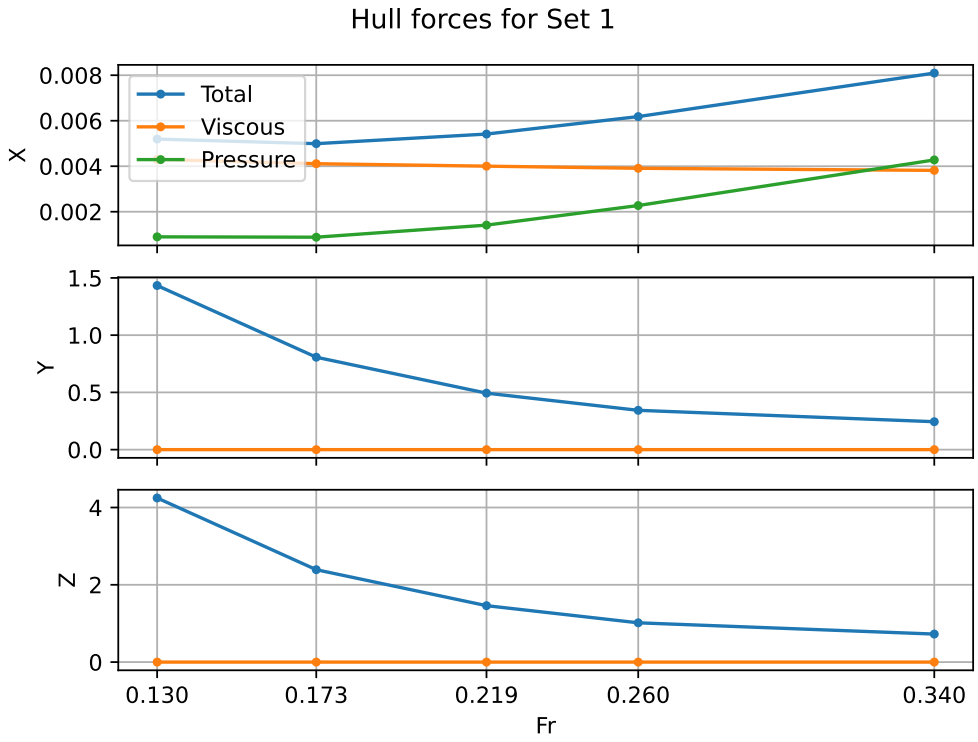

Figure 10 – Predicted resistance, side force and vertical force as a function of the Froude number for the computations in Set 1.

For Set 2, the hull forces are displayed in Fig. 11. As expected, the pressure contribution to the resistance (X) is practically independent of the scale. The viscous contribution shows the familiar scale dependence where at smaller scales, the relative contribution of friction increases as compared to larger scales. For the lateral and vertical hull forces, the viscous contribution is again nearly zero, which means that lateral and vertical force are mostly pressure-based. And as was the case for the resistance component of the hull force, the pressure component is independent of the scale, which means that the total values for the lateral and vertical force components are scale-independent.

4.3 Visualisation of the free surface - Set 1 and 2

The relative wave elevation[3] is shown in Fig. 12 for all compulsory cases in Set 1 and Set 2. The tow row shows the wave pattern at full scale for three different speeds, while the middle column shows the wave pattern at the intermediate speed at four different scales. When the wave elevations at the different lateral

[3] Wave elevation divided by $L_{pp} \times 100$.

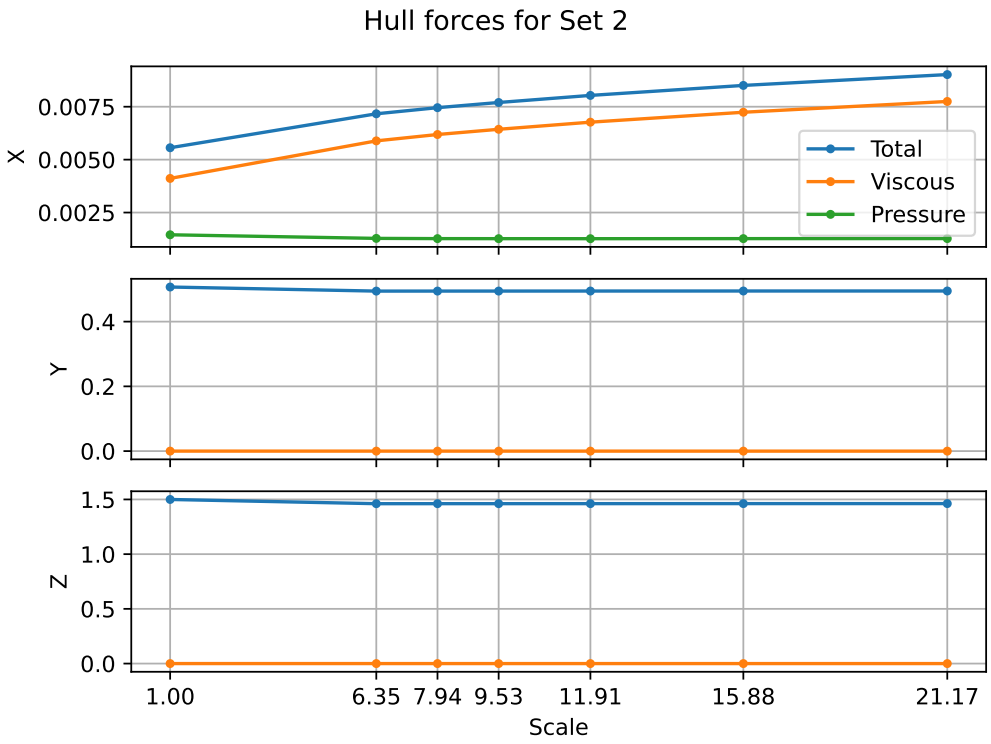

Figure 11 – Predicted resistance, side force and vertical force as a function of the Froude number for the computations in Set 1.

cuts for different ship sizes are compared (Fig. 13), one immediately sees that the secondary wave pattern for $\lambda = 6.35$ is somewhat different from the other submissions. At the time of writing this report, the cause for this difference is unknown.[4]

For the waves generated in the wake of the hull (right-hand side of the upper three graphs in Fig. 13), it is shown that as the model size is reduced further, the differences with the full scale results increase. This is caused by the difference in Reynolds number which affects the magnitude of the viscous component of the results.

[4]A quick check showed that the velocity, scale and turbulence quantities for this computation had the correct values, and that the output was generated at the correct position.

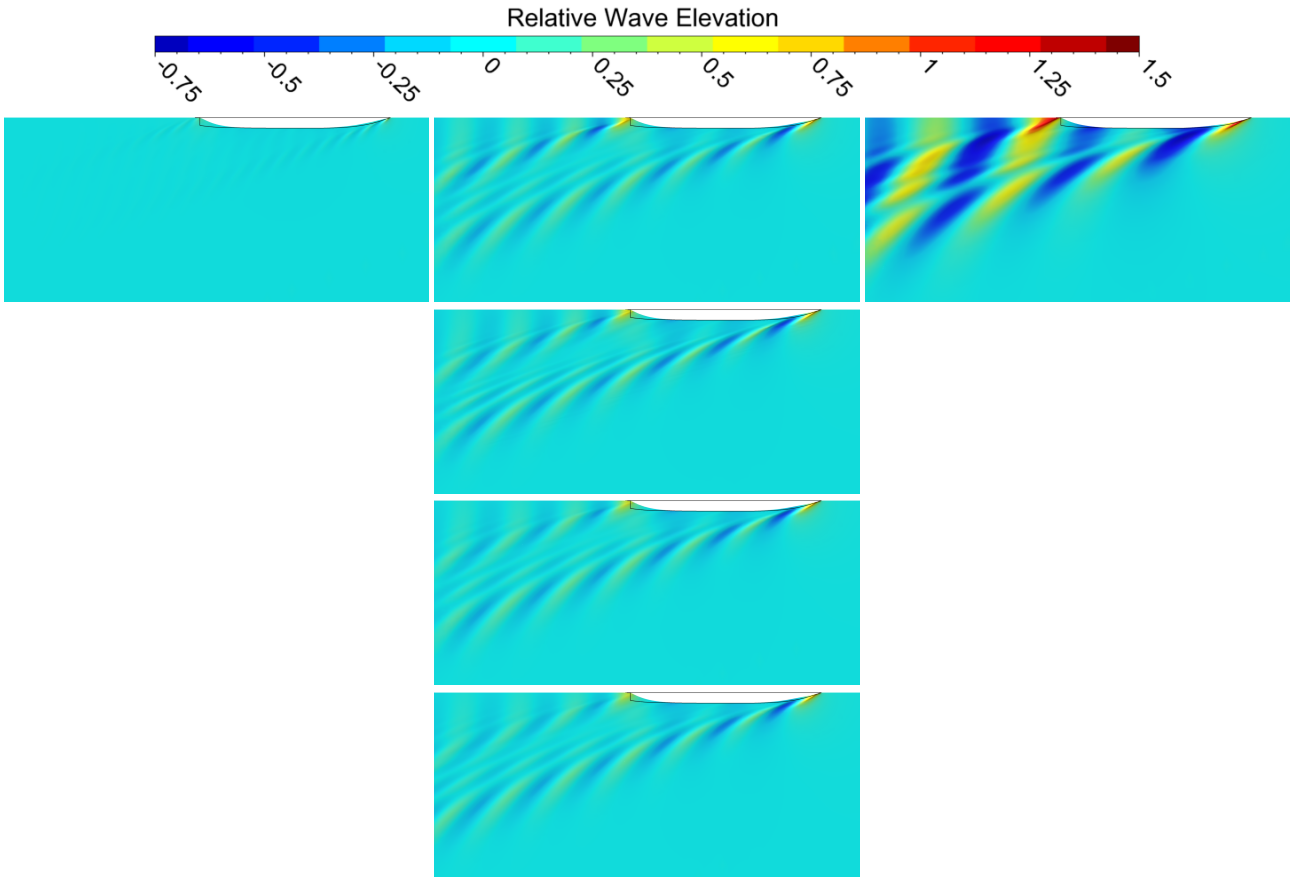

Figure 12 – Relative wave elevations (wave elevation divided by $L_{pp} \times 100$) at full scale for compulsory cases in Set 1 and Set 2.

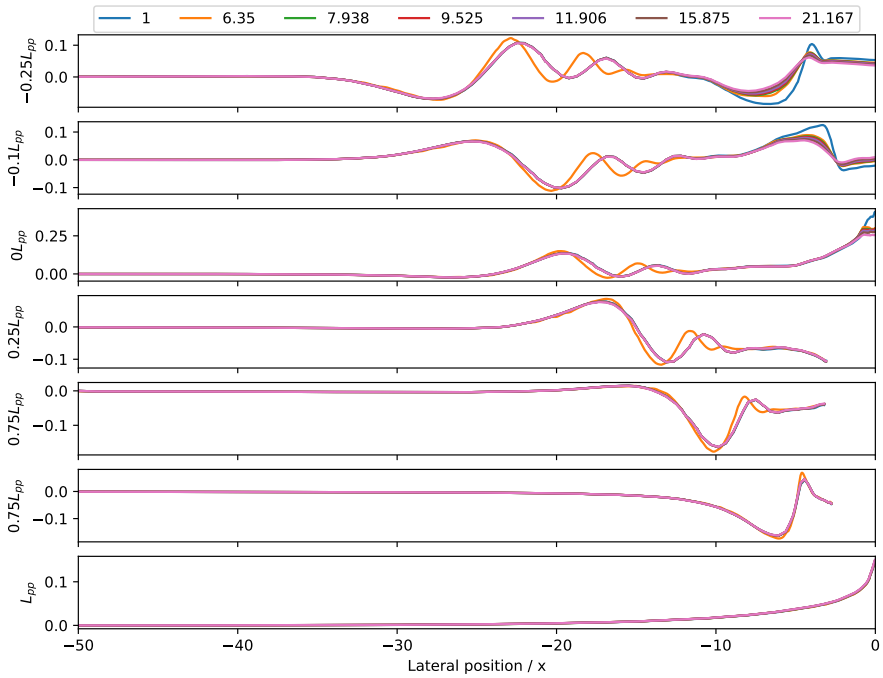

Figure 13 – Comparison of wave cuts at different longitudinal positions for all results at $Fr = 0.219$.

4.4 Set 2 - friction and pressure cuts along hull centreline

For set 2, the friction coefficient and pressure values along the hull centreline are shown in Fig. 14. The friction coefficient results displayed in the top plot clearly show the influence of the Reynolds number on the frictional resistance: at smaller scales, the contribution of frictional resistance is higher. The pressure results have been scaled similarly. There is a noticeable (constant) difference between the full-scale results and the model scale results along almost the entire hull length (except for the bow). Unlike for the frictional resistance values the pressure results at smaller scale more or less overlap.

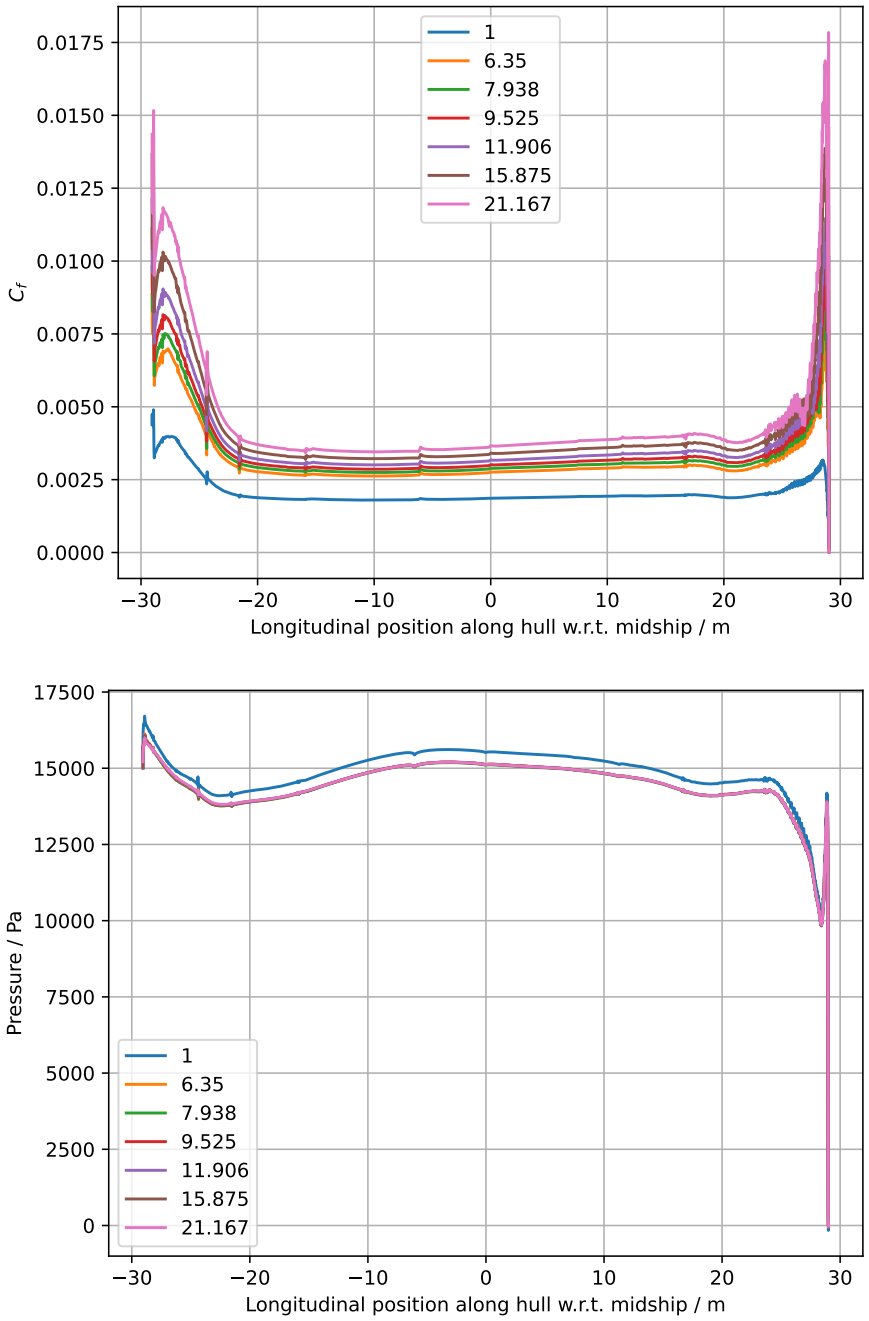

Figure 14 – Comparison of friction coefficient (top) and pressure (bottom) at the hull centreline for all scales at $Fr = 0.219$.

5 Conclusions

Executing doubly body computations on structured grids (with a symmetry plane) in FINE/Marine has proven tricky during the workshop. Initially, the cases were configured as single-phase computations (as they should) but this gave convergence issues with at least one of the computations. The configuration was modified to a two-phase computation where the VOF equation is not solved by setting a negative value for the under-relaxation parameter for the mass fraction. After this change, the computation showed proper convergence. It was therefore decided to run all computations for Set 0 as two-phase computations. After results were submitted to the workshop, Cadence adapted the manual of FINE/Marine to include guidelines for the successful setup of single-phase computations using structured grids. Single-phase computations run with these modifications indeed showed proper convergence which in addition proved to be faster than the two-phase setup.

A comparison of the results between the one-phase and two-phase setup shows that the latter predicts slightly different results for the viscous resistance of the hull, while significant differences were observed for the pressure and total hull resistance. This is caused by the inclusion of the hydrostatic pressure in the two-phase computations.

Due to the issues encountered with the computations in set 0 and the limited amount of time for the execution of this project, less time than anticipated was available for a thorough analysis of all results before submitting them to the workshop organisation. As a consequence, some of the results (such as the hull pressure in set 0) are different from what they should have been.

DEPARTMENT **MOBILITY & PUBLIC WORKS**
Flanders Hydraulics

Berchemlei 115, 2140 Antwerp
T +32 (0)3 224 60 35
F +32 (0)3 224 60 36
waterbouwkundiglabo@vlaanderen.be
www.flandershydraulics.be